Materials Today Energy 22 (2021) 100848

Contents lists available at ScienceDirect

Materials Today Energy

journal homepage: www.journals.elsevier.com/materials-today-energy/

Magnetic energy harvesting of transmission lines by the swinging triboelectric nanogenerator

Zhihao Yuan [a, b], Xuelian Wei [b, c], Xu Jin [a, b], Yanggui Sun [b], Zhiyi Wu [a, b, c, d, *], Zhong Lin Wang [b, c, d, e, **]

[a] Center on Nanoenergy Research, School of Physical Science and Technology, Guangxi University, Nanning, 530004, PR China
[b] Beijing Institute of Nanoenergy and Nanosystems, Chinese Academy of Sciences, Beijing, 100083, PR China
[c] School of Nanoscience and Technology, University of Chinese Academy of Sciences, Beijing, 100049, PR China
[d] CUSTech Institute of Technology, Wenzhou, Zhejiang, 325024, PR China
[e] School of Materials Science and Engineering, Georgia Institute of Technology, Atlanta, GA, 30332-0245, USA

ARTICLE INFO

Article history:
Received 14 August 2021
Accepted 21 August 2021
Available online 27 August 2021

Keywords:
TENG
High voltage transmission line
Altering magnetic field
Anti-fatigued structure
Self-powered system

ABSTRACT

With the development of smart grids, the demand for monitoring the condition of transmission is becoming high. Harvesting magnetic energy of transmission lines is a feasible approach to provide a sustainable power source for condition monitoring sensors. However, energy harvesting methods for transmission lines are constrained by size and service life. We report an antifatigue triboelectric nanogenerator based on a swinging structure (S-TENG) for magnetic energy harvesting. The S-TENG is composed of several magnets attached to a flexible substrate, which is laminated with a sponge layer, a copper film, and a polytetrafluoroethylene film. The laminated layer acts both as a tribo-layer and as a beam. The distinct structure without a stiff termination also avoids vibration fatigue and ensures the efficient contact of triboelectric layers with each other. The S-TENG presents a maximum peak power of 0.78 mW under 30 MΩ loading resistance. This work reveals the potential for harvesting alternating magnetic energy of transmission lines as an energy source for low-power electronic appliances.

1. Introduction

With the progress of technology and the speeding up of industrialization, society requires a significantly higher consumption of power than before [1,2]. As the arteries of a power system, the number of high voltage power transmission pylons rises fast with the rapid expansion of infrastructure. Monitoring the condition of transmission lines is necessary to ensure the safety of electricity, but it is costly. Various sensors have been used to address the long-term sensing needs of transmission lines. Using batteries as the power source of the sensors may curb the long-term operation; instead, environmental energy harvest technology is a promising solution to powering the monitoring system continuously. More harvesters have been developed to harvest energy from power transmission lines, showing potential application prospects in daily life [3]. The electromagnetic, electrostatic, and piezoelectric harvesters have been demonstrated but also have obvious disadvantages [4–6]. For example, the electromagnetic coil must correspond to the range of current intensity of transmission lines, or the coil may emit heat and cause latent danger. The volume of the electrostatic energy harvesters based on the capacitor principle must be large to achieve high output [7,8]. Finally, piezoelectric ceramics may lose piezoelectricity for long-term operation because of their insufficient mechanical durability [9].

In 2012, the Wang group [10–12] proposed a new method by combining triboelectric effect and electrostatic induction to harvest energy. The triboelectric nanogenerator (TENG) has tremendous low cost, lightweight, and easy integration benefits compared with the traditional energy harvesting method. It can easily convert ambient mechanical energy into sustainable electrical energy [13–19]. The energy harvested using the TENG is sufficient to drive many small electronics and make self-powered electronics networks viable [20–23]. Although TENGs based on magnetic materials have been reported to harvest magnetic energy, the hybridized

* Corresponding author. Center on Nanoenergy Research, School of Physical Science and Technology, Guangxi University, Nanning, 530004, PR China.
** Corresponding author. Beijing Institute of Nanoenergy and Nanosystems, Chinese Academy of Sciences, Beijing, 100083, PR China.
E-mail addresses: wuzhiyi@binn.cas.cn (Z. Wu), zlwang@gatech.edu (Z.L. Wang).

https://doi.org/10.1016/j.mtener.2021.100848
2468-6069/

triboelectric-electromagnetic energy harvesters provide a more effective method to harvest magnetic energy [24]. Recently, a high-output magneto-mechano-triboelectric generator has been designed using a cantilever beam and magnets to harvest alternating magnetic energy [25]. Magnets will be agitated and force the cantilever to vibrate at the resonant frequency. Accordingly, two triboelectric layers contact each other with the movement of the cantilever [26]. In addition, multiferroic materials are developed to respond to the stray magnetic field generated from the household appliances, which show a good output performance [27]. Generally, using magnetic materials with stronger magnetism can significantly enhance the output of the TENG [28].

Herein, a swinging TENG (S-TENG) driven by an alternating current magnetic field (50 Hz) of transmission lines is developed for converting magnetic energy into mechanical energy by using magnets. The magnets drive two tribo-layers to agitate, and the TENG can produce electricity through the change in electrical potential induced by mechanical contact and separation. To ensure stable output performance, NdFeB magnets (N35) are adopted. Importantly, putting two layers into the acrylic cavity without the fixed end distinguishes itself from previous TENGs using a cantilever beam. The free motion instead of vibration effectively prevents the tribo-layer from fatigue failure. In addition, the integrated structure makes it easy to install or remove the S-TENG from the pylon. In terms of the output, the S-TENG has shown an open-circuit voltage (V_{oc}), short-circuit current (I_{sc}), and output power of 88 V, 22 μA, and 0.78 mW, respectively. The output is sufficiently strong to light tens of commercial Light Emitting Diodes (LED) and charge a capacitor to power a sensor. A self-powered alarm system has also been built up. The present work proposes a method to harvest the magnetic energy of transmission lines, which broadens the application scenarios of TENGs.

2. Experimental section

Six rectangular acrylic plates were cut by a laser cutter. Then, they were assembled into a box (16 cm × 4 cm × 2 cm). The top layer consisted of a layer of copper (0.03 mm) and a layer of polytetrafluoroethylene (PTFE) (0.03 mm) which were pasted on the sponge (1 mm) substrate successively. The top layer was cut with a dimension of 16 cm × 4 cm. Four circular magnets (NdFeB, N35) with a diameter of 2 cm and a thickness of 0.2 cm were mounted on the layer at 2 cm apart. The bottom layer composed of a layer of copper (0.03 mm) and a layer of nylon (0.03 mm) was pasted on the acrylic (1 mm) substrate in sequence. The bottom layer was connected to the external circuit with two copper wires. Finally, the two layers were packaged in the cuboid acrylic box.

The output performance of the S-TENG was measured using an electrometer (Keithley 6514 System Electrometer) and a data acquisition card (NI PCI-6255). In the experiment, the S-TENG was placed above the copper cable, which was around the alternating magnetic field generated by an alternating current (AC) source (AHY-12 series linear AC adjustable constant current source).

3. Results and discussion

3.1. Construction of the S-TENG and the working mechanism

Various harvesters running on solar energy and wind energy are placed on the pylon among the available energy harvesting technologies. However, the intermittency of sunlight and wind is difficult to meet the demand for a continuous power supply. This study proposes a TENG with a swinging structure driven by magnetic force, which has a good application prospect in the energy harvesting of transmission lines and satisfies the requirements of a continuous operation. The schematic of the S-TENG can be seen in Fig. 1a, composed of the top and the bottom layers. The magnets are stuck on the top layer consisting of a sponge substrate, an electrode, and a PTFE film. The magnets have good magnetic properties and stability (Fig. S1), with a high maximum magnetic energy product of 267.4 kJ/m^3 (about33.6 MGOe), and they hardly demagnetize before reaching the demagnetization temperature (80 °C), which allows the output of the S-TENG not to decrease over a long time. The bottom layer is made up of an acrylic substrate and two electrodes pasted on a nylon film. When the top layer swings under the altering magnetic field because of the opposite magnetic force directions on the left and right sides of the magnets, it alternately contacts the bottom layer (Fig. 1b). All the components are put in an acrylic box, ensuring both layers do not deviate from their original location and guarantee sufficient contact. As illustrated in Fig. 1c, the S-TENG, a small, simple, and low-cost device, can convert magnetic energy into mechanical energy and then convert mechanical energy to electrical energy.

As illustrated in Fig. 2a, the bottom charge transport layer is constituted of left and right halves, and the top charge transport layer alternately contacts and separates from the left and right halves. PTFE and nylon films produce equal positive and negative charges, respectively. The arrows in the pane symbolize the directions of the current. In the initial state, the right side of the top layer tilts, the left side still contacts the left half (state i), and the current will flow from the bottom electrode to the top electrode. Then, the top layer keeps on moving upward, and the left side also separates from the left half ultimately (state ii), resulting in the current flowing from the top electrode to the bottom electrode. Then, the direction of the magnetic field reverses. The right side begins to slump down under the combined gravity and the magnetic force actuation, and it contacts the right half (state iii), which produces a current flowing from the bottom electrode to the top electrode. Before the left side falls, the right side is lifted away (state iv), which generates a current again. Video S1 records the working process. The TENG works in such a continuous cycle and generates an alternating current in an external circuit. In addition, the output voltage is slightly higher than that of the TENG with one electrode on account of the distinct motion state (Fig. S2a), and the output improves with an increase in electrode size (Fig. S2b).

Supplementary video related to this article can be found at https://doi.org/10.1016/j.mtener.2021.100848

To better illustrate the working process of the S-TENG in an alternating magnetic field, COMSOL software based on the finite-element simulation is used to calculate the magnetic force (Fig. 2b). When the upward vertical force component on the left side reaches a maximum, the force on the right side drops down to the minimum. The distribution of magnetic induction lines with the change of motion states is also simulated (see Fig. 2c). Through the magnetic induction line simulation results, the direction of the resultant external force can be determined. In addition, the simulation also reveals that the electric potential between the two electrodes in the open circuit increases as the gap separation expands.

3.2. Output performance of the S-TENG

An output performance test system is built by using an electrometer and a data acquisition card (Fig. 3a). The S-TENG was placed above the copper wire, and the materials of the component of the S-TENG are modified. The PTFE film and the nylon film are chosen as the composition of the charge transport layer because of their positive and negative electron affinities, respectively. The hardness of the substrate is a major element influencing the output performance. By combining the simulation and experiments, the

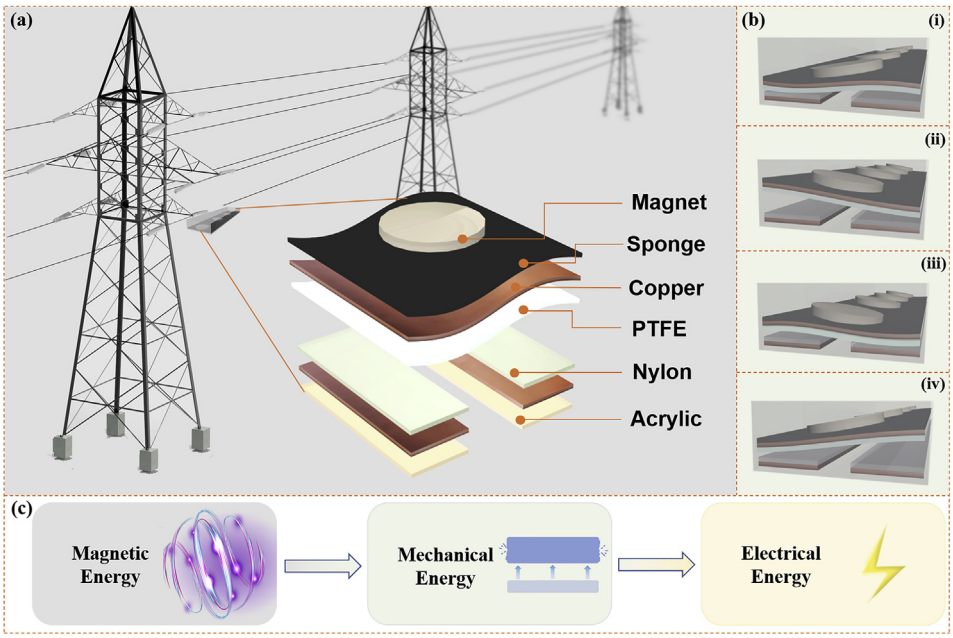

Fig. 1. The schematic diagram of the S-TENG. (a) The structure and working mvechanism of the S-TENG. (b) The working principle of the S-TENG in the magnetic field. (c) The energy conversion process of the S-TENG.

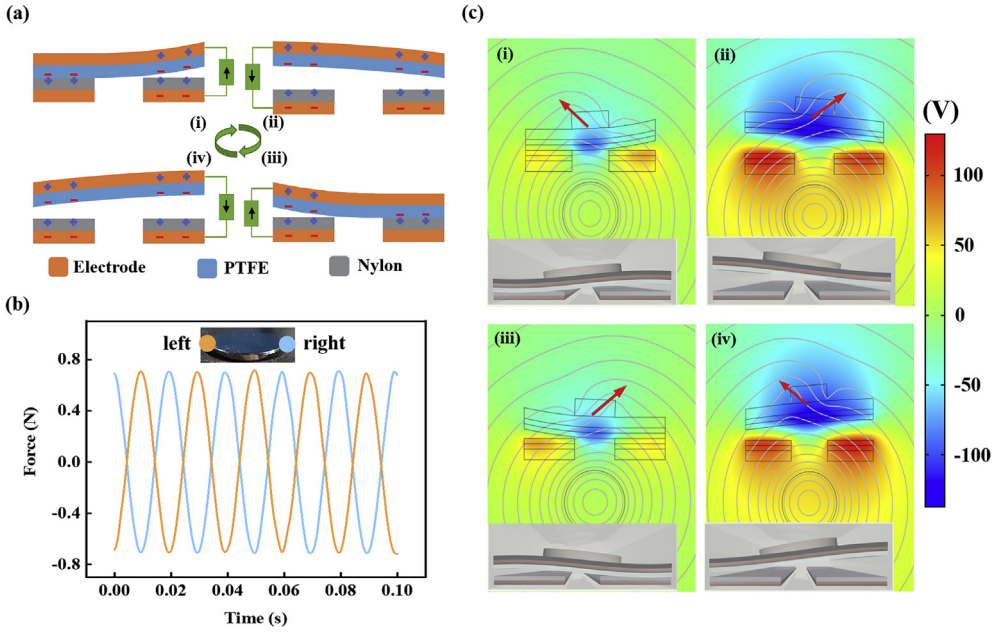

Fig. 2. The working principle of the S-TENG. (a) Schematic of charge distribution. (b) Simulated external force on both sides of the magnet. (c) Electrostatic potential distributions and magnetic induction lines at four typical positions. Insets: sketches of the corresponding motion states (see also photos in Fig. S3).

motion states of the substrate driven by magnets in the magnetic field are shown in Fig. 3b. The substrate swings from one side to the other like a ship shaken by waves. A plate with high hardness cannot achieve high output, such as an acrylic plate. It hardly bends without excessive stress. When the acrylic plate falls, it will form an angle with the bottom layer, which leads to a poor contact situation. Therefore, the substrate needs to be a deformable material in this situation, such as a sponge that shows good mechanical properties. After replacing acrylic material with a sponge of the same weight, the output performance rises highly, but the waveforms are uneven. It could be the use of the beam without a clamped end, which avoids vibration fatigue but at the expense of the stability of the swinging motion. Meanwhile, the falling speed and angle of the magnets may not be the same, and the soft substrate amplifies the difference, leading to the waveform with multiple peaks in a period (Fig. 3c). In summary, the output is considerably improved by the increased contact area of the flexible substrate.

Moreover, the choice of magnets is a critical factor that directly affects the gap separation and potential. The mass of the magnets increases exponentially with the volume. In contrast, the magnetic force does not increase exponentially (Fig.S4) because magnetic induction intensity is not equally distributed around the wire.

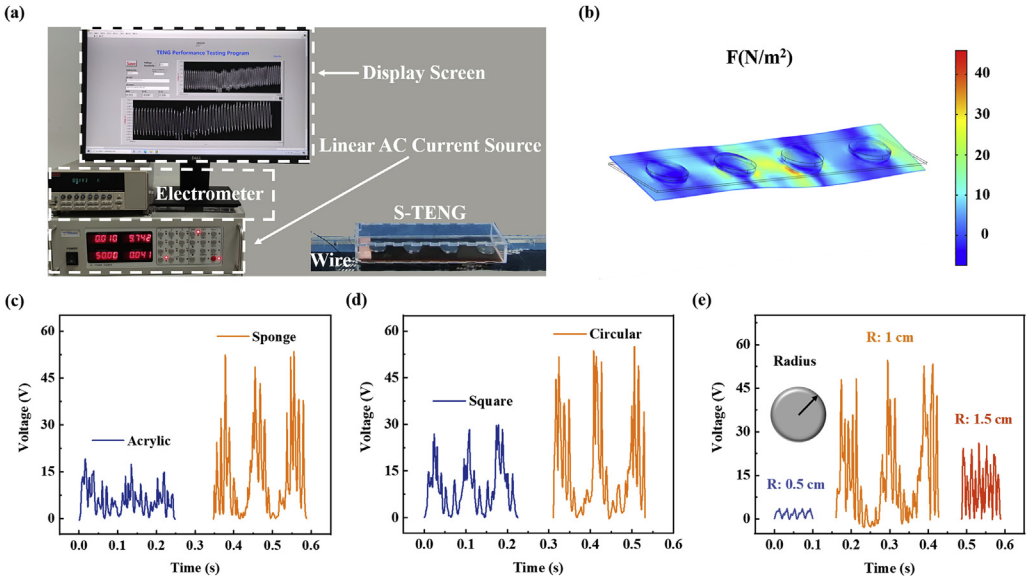

Fig. 3. Effect incurred by changing the magnet and material of the substrate on the output performance of the S-TENG. (a) The photo of the testing system. (b) Simulated motion state of the substrate. (c) V_{oc} under different materials of the substrate. Output performance in magnets with (d) different shapes and (e) different radii and masses.

Therefore, when the magnet material is determined, the magnet with suitable dimensions may obtain an optimal balance between magnetic force and gravity, providing the best motion response and the highest output performance. For the rectangular magnets, more magnetic flux passes through the magnets if the magnets are vertical to the substrate instead of parallel to the substrate. Fig. S5 displays the output under different dimensions of the rectangular magnets. Positioning rectangular magnets perpendicular to the substrate (16 cm × 4 cm), when the current flowing through the wire is 300 A, the output voltage increases first and then decreases with the volume of magnets getting bigger. Owing to the best stress condition when the length and width are equal, the square magnets (2 cm × 2 cm) perform best. For the circular magnets, the output performances of circular magnets ($\Phi = 2$ cm) and square magnets (2 cm × 2 cm) at the current intensity of 300 A are compared (Fig. 3d). Magnets of the same number are used, and the mass of circular magnets (4.71 g) is approximately three-quarters of the square ones (6 g). Surprisingly, the output is nearly twice as high as the square ones because the gap separation of using square magnets is smaller than that of using circular magnets when the current is 300 A. Consequently, circular magnets are selected to obtain better output performance.

The influence of the radius when using circular magnets of the same thickness is shown in Fig. 3e. The magnets with a radius of 1 cm achieve the highest output voltage of 58 V, and the other two radii of circular magnets used in the experiment are not as good as the previous ones. The magnets with a radius of 0.5 cm and 1.5 cm weigh 1.18 g and 10.60 g, respectively. The top layer does not separate from the left and right halves when using magnets with a radius of 0.5 cm, resulting in low output. The waveform is regular because the top layer only vibrates in the alternating magnetic field. Although the magnets with a radius of 1.5 cm attain a certain gap separation, the gap separation is not apparent enough because their quality is more significant. They all fail to achieve a good output performance.

The S-TENGs with different lengths and widths are fabricated to demonstrate the influence of the size. Fig. 4a shows the relationship between the output and length. The optimum extent of the S-TENG is 16 cm. Furthermore, the optimum width of the S-TENG is 4 cm (Fig. 4b). In this situation, the flexible substrate sufficiently enhances the contact of two tribo-layers, leading to the maximum output. Fig. 4c shows the output voltage of the S-TENG under the different distances between the S-TENG and the wire. Distinctly, the increased output can attribute to the stronger magnetic induction intensity with the distance decreasing. The output voltage of the S-TENG gradually enhances as the current intensity increases (Fig. 4d). The substrate only vibrates under the current intensity of 100 A and 200 A, resulting in a regular waveform, and it will not stay flat after it bounces, resulting in an irregular potential change. Fig. 4e investigates the change of output current with different current intensities. The output current reaches a high value when the top layer still contacts the bottom layer, owing to the coupling effect of triboelectrification and electrostatic induction. The waveform also becomes uneven when the top electrode is completely separated from the bottom electrode. The magnetic force and the output current remain on an upward trend, more force accelerates the magnet, and the output current is proportional to the contact/separate velocity. Similarly, the amount of transferred charge shown in Fig. 4f also tends to increase with magnetic field intensity. The output of the S-TENG shows a slight increase as the current intensity increases, which means the S-TENG can maintain a relatively stable output even responding to the dynamic load on the wire.

Besides, a hybridized triboelectric-electromagnetic energy harvester can improve the output further. A coil ($\Phi = 4$ cm) is adhered to the bottom of the S-TENG to harvest the energy under the current intensity of 500 A and the distance between them of 1 cm. Fig. S6 depicts the V_{oc} and I_{sc}. In this situation, coils transform the motion of the permanent magnets into electricity through the electromagnetic induction effect. However, the swing amplitude of magnets is not large enough to form a big angle between two motion states, which leads to a slight variation of magnetic flux with time. There will be a better way to add a coil to improve the output of the hybridized harvester. Changing the position of the coil to the side of the S-TENG, better performance is obtained under the same current intensity and distance. The V_{oc} and I_{sc} (Fig. S7) are much bigger than the previous results. Because the magnetic flux produced by the transmission line passes through the coil

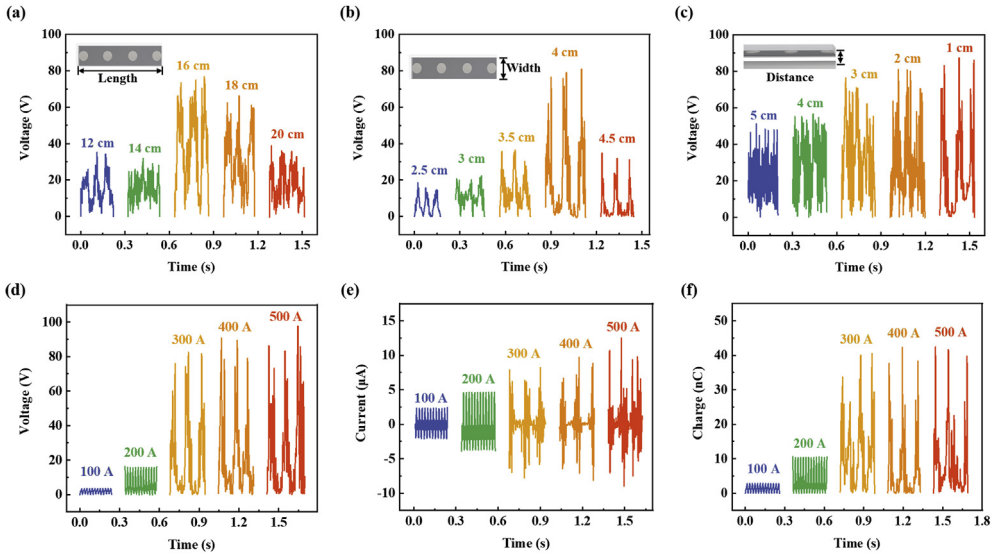

Fig. 4. Output performance of the S-TENG under different smoothing variables. V_{oc} of (a) different lengths, (b) different widths, and (c) different distances between the wires. (d) V_{oc}, (e) I_{sc}, and (f) Q_{tr} under different current intensities.

vertically, by comparison, the impact of the magnets is almost negligible. In addition to adding electromagnetic generator (EMG), connecting several S-TENGs in parallel may also be a good option. Two parallel S-TENGs also improve the output performance significantly (Fig. S8). These ways prove the possibility to enhance the output and expand the potential application of S-TENGs.

3.3. Application demonstration

The peak electrical power produced by the S-TENG is displayed in Fig. 5a when the analog current is at 500 A. The plot represents the output performance under different load resistances. The plot shows that the maximum output power is 0.78 mW at 30 MΩ, and

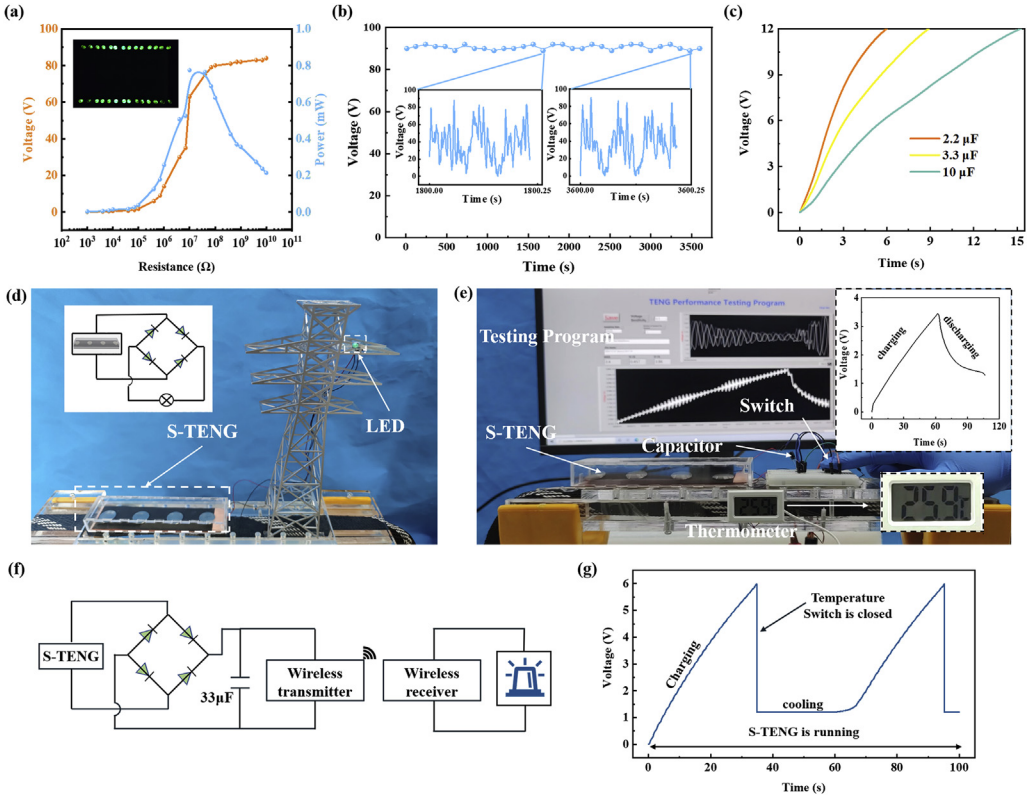

Fig. 5. Application demonstration of the S-TENG. (a) Output performance under different external loads of the S-TENG. Inset: the photo of lighting 24 commercial LEDs. (b) Stability test of the S-TENG for around 180,000 cycles. (c) Charging performances of the S-TENG for various capacitors. (d) The photograph of an LED that is powered by the S-TENG. Inset: the equivalent circuit for powering the LED. (e) The picture of the S-TENG–based temperature sensor. (f) The schematic diagram of a self-powered wireless temperature alarm system. (g) The typical working waveform of the temperature alarm system.

the S-TENG can light up 24 commercial LEDs (inset of Fig. 5a). In addition, the V−Q plots are used to assess quantitative information about the output energy per cycle of the S-TENG (Fig. S9). The area enclosed by this loop is the energy output of the S-TENG per cycle. It can be deduced that output energy per cycle is 1.29 μJ. The unsmooth behavior of the curves is caused by the irregular output curve of the S-TENG. The durability of the S-TENG is also tested (Fig. 5b). The output of the S-TENG is stable after continuous operation for 1 h, about 180,000 cycles. Because the linear current source will heat up after an ongoing operation, which may melt the circuitry or make a short circuit, it cannot operate for a long time. However, electromagnetic heating is not violent enough to affect the continuous work in natural scenes. After testing another S-TENG for a total of 100 h, there is no wrinkle caused by fatigue strain (Fig. S10).

By assembling all the elements in a box, the S-TENG can be easily set up in the alternating magnetic field to harvest energy. The output power can be used to charge different commercial capacitors, as shown in Fig. 5c, in which the 3.3 μF capacitor can be charged to 12 V in 9 s, whereas the 10 μF capacitor needs 12 s. It only takes 6 s to charge the 2.2 μF capacitor to 12 V when the current intensity is 500 A. Even if the intensity of the magnetic field drops down to one twenty-fifth of the initial intensity, output power also charges capacitors fast (Fig. S11). In addition, the S-TENG can power lighting sources and sensors after the current is rectified through the bridge rectifier, as shown by the simulation demonstration model (Fig. 5d and Video S2). Fig. 5e and Video S3 illustrate the whole working process of powering a temperature sensor. The sensor system is made up of a 100 μF capacitor, bridge rectifier, and thermometer. The thermometer is activated when the capacitor is charged from 0 to 3.4 V for 1 min by the S-TENG. Fig. 5f provides the schematic diagram of a self-powered wireless temperature alarm system composed of a temperature switch, a 33 μF capacitor, and an alarm. The magnetic energy harvested by the S-TENG is saved in the capacitor. When the temperature reaches the trigger threshold, the switch will be closed, and the alarm will be activated so that the potential fire disaster will be strangled at birth. Fig. 5g displays the typical working waveform of the system. The capacitor is charged to the operating voltage in 35 s. The alarm system starts to operate when the switch is heated. Video S4 illustrates the complete process. The above mentioned experiments reveal that the S-TENG has great potential application for temperature monitoring and power supply for other electrical appliances.

Supplementary video related to this article can be found at https://doi.org/10.1016/j.mtener.2021.100848

4. Conclusion

In conclusion, an energy harvester composed of magnets and tribo-layers has been proposed to harvest the environmental energy of transmission lines by converting magnetic energy to electrical energy. Permanent magnets act as the driver of the S-TENG to respond to the magnetic field. The structure design without a clamped beam allows swinging of the top layer and avoids vibration fatigue, and the soft sponge substrate enhances the triboelectric contact area. With the tribo-layers and magnets put into an acrylic box, this generator is convenient to install. The output of the S-TENG shows a slight increase after the current reaches 300 A, showing the production of the S-TENG does not fluctuate with the dynamic current on transmission lines. We demonstrate that the S-TENG can fast charge a capacitor and power a thermometer constantly. A self-powered wireless temperature alarm system has also been fabricated successfully, illustrating its application potential in smart sensors.

Credit author statement

Zhihao Yuan: Conceptualization, Data curation, Methodology, Visualization, Writing - original draft. **Xuelian Wei:** Writing - review & editing. **Xu Jin:** Investigation, Methodology. **Yanggui Sun:** Writing - review & editing. **Zhiyi Wu:** Conceptualization, Methodology, Formal analysis, Writing - review & editing. **Zhong Lin Wang:** Supervision.

Author contributions

All authors have given approval to the final version of the manuscript.

Funding sources

The research was supported by the National Key R&D Program of China (2016YFA0202703).

Declaration of competing interest

The authors declare that they have no known competing financial interests or personal relationships that could have appeared to influence the work reported in this paper.

Appendix A. Supplementary data

Supplementary data to this article can be found online at https://doi.org/10.1016/j.mtener.2021.100848.

References

[1] Z.L. Wang, Triboelectric nanogenerators as new energy technology and self-powered sensors - principles, problems and perspectives, Faraday Discuss 176 (2014) 447−458, https://doi.org/10.1039/c4fd00159a.
[2] Z.L. Wang, Entropy theory of distributed energy for internet of things, Nanomater. Energy 58 (2019) 669−672, https://doi.org/10.1016/j.nanoen.2019.02.012.
[3] M. El Ganaoui, M. El Jouad, R. Bennacer, J.-M. Nunzi, Advanced materials for energy harvesting, storage, sensing and environmental engineering II, Eur. Phys. J. Appl. Phys. 93 (2021) 10902, https://doi.org/10.1051/epjap/2020200364.
[4] S. Du, Y. Jia, A.A. Seshia, An efficient inductorless dynamically configured interface circuit for piezoelectric vibration energy harvesting, IEEE Trans. Power Electron. 32 (2017) 3595−3609, https://doi.org/10.1109/tpel.2016.2587757.
[5] J. Leicht, Y. Manoli, A 2.6 mu W-1.2 mW autonomous electromagnetic vibration energy harvester interface IC with conduction-angle-controlled MPPT and up to 95% efficiency, IEEE J. Solid State Circ. 52 (2017) 2448−2462, https://doi.org/10.1109/jssc.2017.2702667.
[6] H.-C. Song, P. Kumar, D. Maurya, M.-G. Kang, W.T. Reynolds Jr., D.-Y. Jeong, C.-Y. Kang, S. Priya, Ultra-low resonant piezoelectric MEMS energy harvester with high power density, J. Microelectromech. Syst. 26 (2017) 1226−1234, https://doi.org/10.1109/jmems.2017.2728821.
[7] D. Mallick, P. Constantinou, P. Podder, S. Roy, Multi-frequency MEMS electromagnetic energy harvesting, Sensor Actuator Phys. 264 (2017) 247−259, https://doi.org/10.1016/j.sna.2017.08.002.
[8] Z. Wu, Y. Wen, P. Li, A power supply of self-powered online monitoring systems for power cords, IEEE Trans. Energy Convers. 28 (2013) 921−928, https://doi.org/10.1109/tec.2013.2281075.
[9] J.H. Lee, J.Y. Park, E.B. Cho, T.Y. Kim, S.A. Han, T.H. Kim, Y. Liu, S.K. Kim, C.J. Roh, H.J. Yoon, H. Ryu, W. Seung, J.S. Lee, J. Lee, S.W. Kim, Reliable piezoelectricity in bilayer WSe2 for piezoelectric nanogenerators, Adv. Mater. 29 (2017) 1606667, https://doi.org/10.1002/adma.201606667.
[10] Z.L. Wang, Triboelectric nanogenerators as new energy technology for self-powered systems and as active mechanical and chemical sensors, ACS Nano 7 (2013) 9533−9557, https://doi.org/10.1021/nn404614z.
[11] Z.L. Wang, J. Chen, L. Lin, Progress in triboelectric nanogenerators as a new energy technology and self-powered sensors, Energy Environ. Sci. 8 (2015) 2250−2282, https://doi.org/10.1039/c5ee01532d.
[12] J. Shao, T. Jiang, Z. Wang, Theoretical foundations of triboelectric nanogenerators (TENGs), Sci. China Technol. Sci. 63 (2020) 1087−1109, https://doi.org/10.1007/s11431-020-1604-9.
[13] S.P. Beeby, M.J. Tudor, N.M. White, Energy harvesting vibration sources for microsystems applications, Meas. Sci. Technol. 17 (2006) R175−R195, https://doi.org/10.1088/0957-0233/17/12/r01.

[14] Z. Deng, M.J. Dapino, Review of magnetostrictive vibration energy harvesters, Smart Mater. Struct. 26 (2017) 103001, https://doi.org/10.1088/1361-665X/aa8347.
[15] W. Li, N. Wu, J. Zhong, Q. Zhong, S. Zhao, B. Wang, X. Cheng, S. Li, K. Liu, B. Hu, J. Zhou, Theoretical study of cellular piezoelectret generators, Adv. Funct. Mater. 26 (2016) 1964–1974, https://doi.org/10.1002/adfm.201503704.
[16] S. Lu, Q. Liao, J. Qi, S. Liu, Y. Liu, Q. Liang, G. Zhang, Y. Zhang, The enhanced performance of piezoelectric nanogenerator via suppressing screening effect with Au particles/ZnO nanoarrays Schottky junction, Nano Res. 9 (2016) 372–379, https://doi.org/10.1007/s12274-015-0916-6.
[17] Y. Qin, X. Wang, Z.L. Wang, Microfibre-nanowire hybrid structure for energy scavenging, Nature 451 (2008), https://doi.org/10.1038/nature06601. 809-U805.
[18] N. Wu, X. Cheng, Q. Zhong, J. Zhong, W. Li, B. Wang, B. Hu, J. Zhou, Cellular polypropylene piezoelectret for human body energy harvesting and health monitoring, Adv. Funct. Mater. 25 (2015) 4788–4794, https://doi.org/10.1002/adfm.201501695.
[19] B.K. Zeeshan, R. Panigrahi, M.U. Ahmed, J.C. Mehmood, Y. Park, W. Chun Kim, Operation of a low-temperature differential heat engine for power generation via hybrid nanogenerators, Appl. Energy 285 (2021) 116385, https://doi.org/10.1016/j.apenergy.2020.116385.
[20] N. Cui, J. Liu, L. Gu, S. Bai, X. Chen, Y. Qin, Wearable triboelectric generator for powering the portable electronic devices, ACS Appl. Mater. Interfaces 7 (2015) 18225–18230, https://doi.org/10.1021/am5071688.
[21] H. Guo, X. He, J. Zhong, Q. Zhong, Q. Leng, C. Hu, J. Chen, L. Tian, Y. Xi, J. Zhou, A nanogenerator for harvesting airflow energy and light energy, J. Mater. Chem. 2 (2014) 2079–2087, https://doi.org/10.1039/c3ta14421f.
[22] M. Sahu, S. Hajra, J. Bijelic, D. Oh, I. Djerdj, H.J. Kim, Triple perovskite-based triboelectric nanogenerator: a facile method of energy harvesting and self-powered information generator, Mater. Today Energy 20 (2021) 100639, https://doi.org/10.1016/j.mtener.2021.100639.
[23] M. Wu, Z. Gao, K. Yao, S. Hou, Y. Liu, D. Li, J. He, X. Huang, E. Song, J. Yu, X. Yu, Thin, soft, skin-integrated foam-based triboelectric nanogenerators for tactile sensing and energy harvesting, Mater. Today Energy 20 (2021) 100657, https://doi.org/10.1016/j.mtener.2021.100657.
[24] Z. Wu, H. Guo, W. Ding, Y.C. Wang, L. Zhang, Z.L. Wang, A hybridized triboelectric-electromagnetic water wave energy harvester based on a magnetic sphere, ACS Nano 13 (2019) 2349–2356, https://doi.org/10.1021/acsnano.8b09088.
[25] K.-W. Lim, M. Peddigari, C.H. Park, H.Y. Lee, Y. Min, J.-W. Kim, C.-W. Ahn, J.-J. Choi, B.-D. Hahn, J.-H. Choi, D.-S. Park, J.-K. Hong, J.-T. Yeom, W.-H. Yoon, J. Ryu, S.N. Yi, G.-T. Hwang, A high output magneto-mechano-triboelectric generator enabled by accelerated water-soluble nano-bullets for powering a wireless indoor positioning system, Energy Environ. Sci. 12 (2019) 666–674, https://doi.org/10.1039/c8ee03008a.
[26] J. Chen, H. Guo, Z. Wu, G. Xu, Y. Zi, C. Hu, Z.L. Wang, Actuation and sensor integrated self-powered cantilever system based on TENG technology, Nanomater. Energy 64 (2019) 103920, https://doi.org/10.1016/j.nanoen.2019.103920.
[27] S. Hajra, V. Vivekananthan, M. Sahu, G. Khandelwal, N.P.M. Joseph Raj, S.-J. Kim, Triboelectric nanogenerator using multiferroic materials: an approach for energy harvesting and self-powered magnetic field detection, Nanomater. Energy 85 (2021) 105964, https://doi.org/10.1016/j.nanoen.2021.105964.
[28] H. Wu, A. Tatarenko, M.I. Bichurin, Y. Wang, A multiferroic module for biomechanical energy harvesting, Nanomater. Energy 83 (2021) 105777, https://doi.org/10.1016/j.nanoen.2021.105777.